# Drone-Small-Cell-Assisted Spectrum Management for 5G and Beyond Vehicular Networks

Hang Shen*, Yilong Heng*, Ning Shi†, Tianjing Wang*, Guangwei Bai*

*College of Computer Science and Technology, Nanjing Tech University, Nanjing 211816, China
†Nanjing Trusted Blockchain and Algorithm Economics Institute, Nanjing 211899, China
{hshen, wangtianjing, bai}@njtech.edu.cn, shining@newspiral.net

*Abstract*—With advancements in cellular vehicle-to-everything (C-V2X) and drone manufacturing technologies, integrating drone-small-cells (DSCs) into terrestrial cellular networks is a promising solution to enabling diversified vehicle applications. In this paper, a multi-DSC-assisted dynamic spectrum management framework is presented to maximize the network utility under quality-of-service (QoS) constraints in 5G and beyond cellular vehicular networks. The network utility maximization problem is formulated as mixed-integer nonlinear programming regarding association patterns between vehicles and base stations (BSs) and spectrum partitioning among heterogeneous BSs. For mathematical tractability, the joint optimization problem for spectrum partitioning and vehicle-DSC associations is transformed as a biconcave optimization problem. An alternate search algorithm is then designed to determine vehicle association patterns and spectrum slicing ratios. Our simulation demonstrates that compared with state-of-the-art methods, the proposed scheme achieves a significant performance improvement in network throughput and spectrum utilization.

*Index Terms*—Vehicular networks, drone-small-cell, spectrum slicing, resource allocation, QoS-guarantee

## I. INTRODUCTION

As one of the typical fifth-generation (5G) and beyond scenarios, vehicular networks connect vehicles, sensors, pedestrians, mobile devices, and base stations (BSs), providing high definition map and cruise control information to autonomous vehicles for road safety and traffic management [1]. Underpinned by 5G and beyond networks, cellular vehicle-to-everything (C-V2X) provides low-latency, high-reliability, and high throughput communications for various services and support massive interconnected vehicle access [2].

Drones equipped with specific wireless transceivers can form drone-small-cells (DSCs) that cooperate with ground base stations (GBSs). Air-ground integrated networks have become a promising architecture for ubiquitous connectivity for 5G and Beyond, with great potential to improve the performance of vehicular networks [3]. First, with the advantage of flying height, DSCs can avoid the shadow fading in data transmission and has a higher probability of establishing a short-distance line of sight (LoS) communication link with reduced delay and

increased reliability [4]. Second, DSC relays can extend the coverage of infrastructures and relieve the resource allocation pressure for vehicles at GBS edge areas. Third, due to the low transmit power and adjustable deployment, introducing DSCs underlaying GBSs can facilitate spectrum reuse.

However, spectrum management in air-ground integrated vehicular networks faces many challenging problems. First, due to GBS-to-DSC (G2D) and DSC-to-vehicle (D2V) channels' uniqueness, a performance trade-off exists between effective coverage and spectrum utilization in DSC deployment. Second, due to DSCs' maneuverability, vehicle-BS and DSC-GBS association patterns become diverse, complicating spectrum partitioning among heterogeneous BSs. Third, in spectrum sharing, interference fluctuations accompany DSCs' position adjustment [5]. Therefore, it is imperative to explore flexible BS coverage and efficient spectrum resource provisioning to support emerged applications.

### A. Prior Work and Motivation

A lot of resource management methods for terrestrial vehicular networks have been proposed by researchers. Peng *et al.* design a joint power control and resource allocation strategy to provides QoS-guaranteed downlink transmissions in multi-access edge computing (MEC) enabled vehicular networks [6]. They further propose a multi-dimensional resource management framework to maximize the number of offloaded tasks under heterogeneous QoS requirements [7]. A multi-timescale radio access network slicing and task offloading problem is investigated in [8], aiming to maximize resource utilization with diverse QoS guarantee for autonomous driving tasks.

How to deploy and move DSCs is critical to service provisioning. Reference [9] derives the drone flight altitude that maximizes ground coverage, considering path loss and urban environmental statistical parameters. Sun *et al.* deduce the spectrum efficiency at end devices and study how to improve resource utilization via DSC deployment [10]. Shi *et al.* develop a drone ground coverage model to formulate the drone 3D deployment problem, intending to maximize end device coverage subject to the drone-to-ground link quality constraint [11]. However, the impact of drone flight height on resource consumption and network coverage needs further investigation. A drone-assisted cellular networking scheme is proposed in [12] to improve coverage for machine-type communication services.

Relatively little literature focuses on resource management in DSC-assisted vehicular networks. Zhang *et al.* propose a software-defined networking (SDN)-based resource management architecture for air-space-ground integrated vehicular networks [13], where local and centralized controllers cooperate to manage resources. He *et al.* investigate the drone relay selection problem [14], considering the influence of communication interruption probability and transmission energy consumption. Wu *et al.* investigate a space-air-ground integrated framework for efficient network slicing and content services for vehicular networks [15]. Lvy *et al.* present a service-oriented resource slicing framework for space-air-ground integrated vehicular networks to maximize the system revenue and stabilize the time-averaged queue [16].

Some issues require further investigation:

- Some research assumes that DSCs can provide services to vehicles without GBSs' support and ignore the resource consumption of DSC-to-GBS communications;
- Dynamically slicing spectrum resources among heterogeneous BSs should consider the vehicle services' traffic features and distinctive drone channels.

### B. Contributions and Organization

Considering a scenario where multiple DSCs and multiple GBSs coexist, we propose an air-ground integrated spectrum management framework for 5G and beyond cellular vehicular networks, focusing on maximizing network utility while satisfying QoS requirements. The main contributions include:

- An optimization framework for spectrum partitioning among heterogeneous BSs is developed, with the consideration of vehicle location, DSC deployment, traffic statistics, QoS requirements, and inter-DSC interference;
- Using logarithmic and linear utility functions, we formulate a utility maximization problem to determine spectrum slicing ratios and vehicle-BS association patterns;
- The optimization problem is transformed into a tractable biconcave maximization problem regarding spectrum partitioning and device association patterns. A convex search algorithm is developed to obtain partial optimal solutions. Simulation results show that the proposed method outperforms the existing benchmark methods.

The follow-up content is arranged in following sections. The system model under consideration is presented in Section II. The optimization problem formulation and decomposition are given in Section III. In Section IV, the optimization problem is transformed to a tractable biconcave problem, and an alternate algorithm is proposed to solve the transformed problem. Performance evaluation is presented in Section V, followed by a conclusion in Section VI. Proof of the propositions and corollaries are given in appendices.

## II. SYSTEM MODEL

Consider a two-tier vehicular network with multiple GBSs underlaid by multiple DSCs as shown in Fig. 1. DSCs deploy and move along a preset trajectory, and can forward GBSs' traffic to target vehicles. When not covered by DSCs, a vehicle
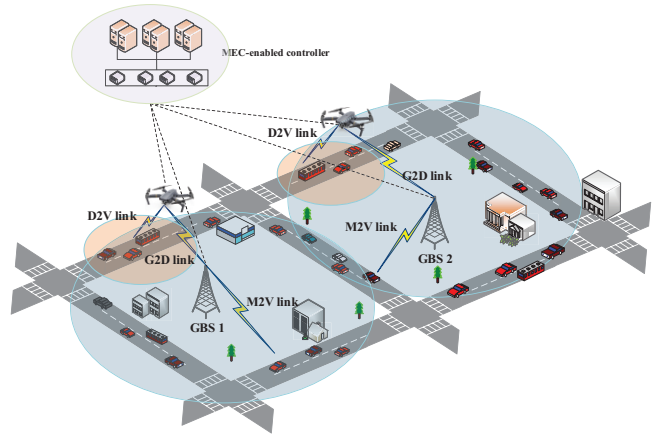


Fig. 1. Drone-small-cell-assisted cellular vehicular networks.
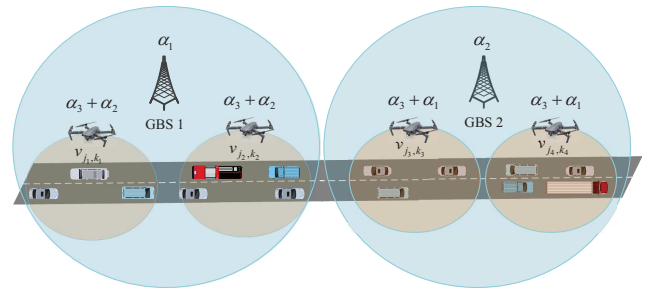


Fig. 2. Spectrum management framework.

chooses to connect to a GBS that covers it. Under the coverage of a DSC, a vehicle can choose to connect to the DSC or a GBS. The physical radio resources from GBSs and DSCs are abstracted as a centralized virtual radio resource pool [17]. By collecting vehicles' request information, a MEC-enabled controller performs joint management.

### A. Spectrum Slicing Framework

GBSs are divide into two groups, denoted by $\mathcal{M}_1$ and $\mathcal{M}_2$, where GBSs in the same group share the same spectrum resources and are not adjacent to each other. Take a two-way lane scenario shown in Fig. 2 as an example. GBS 1 and GBS 2 are two GBSs from groups $\mathcal{M}_1$ and $\mathcal{M}_2$, respectively. Without loss of generality, we consider slicing the spectrum resources among GBS 1, GBS 2, and each DSC. The total available amount of radio spectrum resources to the system is denoted as $W$. Assume that spectrum resources is reused by each DSC to support D2V communications under a distance constraint among DSCs. Then, the spectrum resources are divided into three mutually orthogonal spectrum slices, with slicing ratios $\alpha_1$, $\alpha_2$, and $\alpha_3$, and are allocated to GBS 1, GBS 2, and each DSC, satisfying

$$\sum_{n\in\{1,2,3\}} \alpha_n = 1. \tag{1}$$

Denote $v_{j,k} = (x_j, y_j, z_k)$ as a drone deployment position. The set of drone deployment positions under the coverage

of GBS $m$ is denoted as $\mathcal{V}_m$ with $V_m$ being its cardinality (i.e., the number of available DSCs). The fraction of resources from $\alpha_m$ allocated to associated vehicles to support GBS-to-vehicle (G2V) communications is denoted as $\delta_m$. The fraction of resources from $\alpha_m$ allocated to the DSC associated with GBS $m$ at $v_{j,k} \in \mathcal{V}_m$ for G2D communications is denoted as $\delta_{j,k,m}$ ($m \in \{1,2\}$). The slicing ratios satisfy

$$\alpha_m = \delta_m + \sum_{v_{j,k} \in \mathcal{V}_m} \delta_{j,k,m}, m \in \{1,2\}. \tag{2}$$

In addition to reusing resources $W\alpha_3$ among DSCs, we allow the DSCs not covered by a GBS to reuse the GBS's spectrum. Take Fig. 2 as an example. The DSCs at $v_{j_1,k_1}$ and $v_{j_2,k_2}$ can reuse spectrum resource $(\alpha_3 + \alpha_2)W$ and the DSCs at $v_{j_3,k_3}$ and $v_{j_4,k_4}$ can reuse $(\alpha_3 + \alpha_1)W$.

After slicing the spectrum resources, the controller allocates the slices to each BS. The resources in each slice is further partitioned among associated vehicles.

### B. Communication Model

The vehicle set under the coverage of GBS $m$ is denoted by $\mathcal{I}_m$. Based on the proposed spectrum management framework, vehicle $i \in \mathcal{I}_1$ experiences two kinds of interference: from transmissions of other GBSs in $\mathcal{M}_1$ and of DSCs under the coverage of GBSs in $\mathcal{M}_2$. Let $p_m$ and $p_{j,k}$ represent the transmit power of GBS $m$ and the DSC at $v_{j,k}$. The spectral efficiency at vehicle $i \in \mathcal{I}_1$ from GBS 1 is expressed as

$$r_{i,1} = \log_2\left(1 + \frac{p_1 g_{i,1}}{\sum\limits_{m \in \mathcal{M}_1 \setminus \{1\}} p_m g_{i,m} + \sum\limits_{v_{j,k} \in \mathcal{V}_2} p_{j,k} g_{i,j,k} + \sigma^2}\right) \tag{3}$$

where $\sigma^2$ is the average background noise power and $g_{i,m}$ is the path-loss from GBS $m$ destined for vehicle $i$ as in [18]. Similarly, the spectrum efficiency at vehicle $i \in \mathcal{I}_2$ from GBS 2, $r_{i,2}$, can be obtained. The achievable transmission rates of vehicle $i$ associated with GBS $m$ can be expressed as

$$c_{i,m} = f_{i,m} r_{i,m} \tag{4}$$

where $f_{i,m}$ is the amount of spectrum (out of $\delta_m W$) allocated to vehicle $i$ from GBS $m$.

With the introduction of LoS probability, we characterize the drone channel. Compared with a non-LoS connection, an LoS connection has less attenuation, which improves spectrum efficiency. According to the aerial channel model proposed in [9], [10], the LoS probability of the D2V link from a DSC at $v_{j,k}$ to vehicle $i$ is expressed as

$$P_{\text{LoS}}(z_j, d_{i,j}) = \frac{1}{1 + e_1 \exp\left(-e_2\left(\arctan\left(\frac{z_k}{d_{i,j}}\right)\right) - e_1\right)} \tag{5}$$

where $d_{i,j}$ is the horizontal distance between vehicle $i$ and $v_{j,k}$, $e_1$ and $e_2$ are constants determined by the environment. Based on [10], the average pathloss of the D2V link form the

DSC at $v_{j,k}$ to vehicle $i$ is expressed as

$$g_{i,j,k} = 20 \log \sqrt{z_k^2 + d_{i,j}^2} + (\eta_{\text{LoS}} - \eta_{\text{NLoS}}) P_{\text{LoS}}(z_k, d_{i,j})$$
$$+ 20 \log\left(\frac{4\pi\rho}{c}\right) + \eta_{\text{NLoS}}. \tag{6}$$

In (6), $\eta_{\text{LoS}}$ ($\eta_{\text{NLoS}}$) is the additional loss for LoS (NLoS) links, involving the impacts of shadowing components, $c$ represents the speed of light, and $\rho$ is the carrier frequency.

For the DSC at $v_{j,k} \in \mathcal{V}_1$, let $f_{i,j,k}^{(2)}$ and $f_{i,j,k}^{(3)}$ be the amount of spectrum allocated to vehicle $i$ out of $\alpha_2 W$ and $\alpha_3 W$. The spectrum efficiency at vehicle $i$ with D2V communications include two parts in terms of $f_{i,j,k}^{(2)}$ and $f_{i,j,k}^{(3)}$, expressed as

$$r_{i,j,k}^{(2)} =$$
$$\log_2\left(1 + \frac{p_{j,k} g_{i,j,k}}{\sum\limits_{m \in \mathcal{M}_1} p_m g_{i,m} + \sum\limits_{v_{j',k'} \in \mathcal{V}_1 \setminus \{v_{j,k}\}} p_{j',k'} g_{i,j',k'} + \sigma^2}\right) \tag{7}$$

and

$$r_{i,j,k}^{(3)} = \log_2\left(1 + \frac{p_{j,k} g_{i,j,k}}{\sum\limits_{m \in \{1,2\}} \sum\limits_{v_{j',k'} \in \mathcal{V}_m \setminus \{v_{j,k}\}} p_{j',k'} g_{i,j',k'} + \sigma^2}\right). \tag{8}$$

The achievable transmission rate of vehicle $i$ associated with the DSC at $v_{j,k} \in \mathcal{V}_1$ is the summation of $c_{i,j,k}^{(2)} = f_{i,j,k}^{(2)} r_{i,j,k}^{(2)}$ and $c_{i,j,k}^{(3)} = f_{i,j,k}^{(3)} r_{i,j,k}^{(3)}$. Similarly, denote $f_{i,j,k}^{(1)}$ as the amount of spectrum allocated to vehicle $i$ associated with the DSC at $v_{j,k}$ from $\alpha_1 W$ by the DSC at $v_{j,k}$ under the coverage of GBS 2 ($v_{j,k} \in \mathcal{V}_2$). Then, similar to (7) and (8), the two parts of spectrum efficiencies at the vehicle from the DSC under the coverage of GBS 2, i.e., $r_{i,j,k}^{(1)}$ and $r_{i,j,k}^{(3)}$, can be obtained, and the achievable transmission rate of vehicle $i$ associated with the DSC at $v_{j,k}$ is the summation of $c_{i,j,k}^{(1)} = f_{i,j,k}^{(1)} r_{i,j,k}^{(1)}$ and $c_{i,j,k}^{(3)} = f_{i,j,k}^{(3)} r_{i,j,k}^{(3)}$. If a DSC is associated with GBS $m$, indication variable $b_{j,k,m}$ is set to 1; otherwise 0. Accordingly, given $b_{j,k,1}$ and $a_{j,k,2}$, the achievable transmission rates of vehicle $i$ associated with the DSC at $v_{j,k}$ can be expressed as

$$c_{i,j,k} = b_{j,k,1} c_{i,j,k}^{(2)} + b_{j,k,2} c_{i,j,k}^{(1)} + b_{j,k,1} c_{i,j,k}^{(3)} + b_{j,k,2} c_{i,j,k}^{(3)}. \tag{9}$$

Let $d_{j,k,m} = \sqrt{(x_j - x_m)^2 + (y_j - y_m)^2 + (z_k - z_m)^2}$ be the distance between $v_{j,k}$ and GBS $m$, where $(x_m, y_m, z_m)$ represents the three-dimensional coordinates of GBS $m$. Since DSC flying height is usually higher than that of a GBS, the G2D link is an LoS connection. Denote $\gamma$, $\theta_0$, $\eta_0$ as the terrestrial path-loss exponent, angle offset, and excess path-loss offset. Denote $o_1$ and $o_2$ as excess pathloss scalar and angle scalar. The average path loss from GBS $m$ to $v_{j,k}$ is [19]

$$s_{j,k,m} = 10\gamma \log(d_{j,k,m}) + o_1(\theta - \theta_0) \exp\left(\frac{\theta - \theta_0}{o_2}\right) + \eta_0 \tag{10}$$

where $\theta = \arctan\left(\frac{|z_k - z_m|}{d_{j,k,m}}\right)$ represents the elevation angle
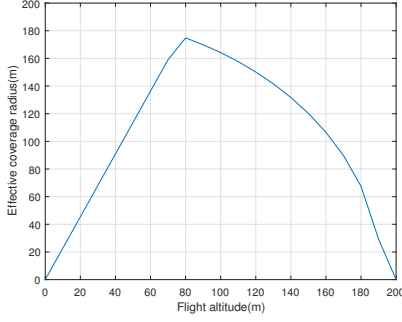
Fig. 3. Impact of flight altitude on effective coverage radius.

between the antennas of the DSC at $v_{j,k}$ and GBS $m$. Similar to (3), the DSC at $v_{j,k}$ associated with GBS 1 experiences two kinds of interference. Then, the spectral efficiency from GBS 1 destined for the DSC at $v_{j,k}$ is expressed as

$$
r_{j,k,1} =
$$
$$
\log_2 \left( 1 + \frac{p_1 s_{j,k,1}}{\sum\limits_{m \in \mathcal{M}_1 \setminus \{1\}} p_m g_{i,m} + \sum\limits_{v_{j,k} \in \mathcal{V}_2} p_{j,k} g_{i,j,k} + \sigma^2} \right) \tag{11}
$$

The spectral efficiency from GBS 2 destined for the DSC at $v_{j,k}$ can be obtained in the same way.

Denote $f_{i,j,k,m}$ as the resources (out of $\delta_{j,k,m} W$) allocated to vehicle $i$ from GBS $m$. When GBS $m$ selects a DSC at $v_{j,k}$ to relay data to vehicle $i$, the achievable transmission rate at the DSC at $v_{j,k}$ can be uniformly expressed as

$$
c_{i,j,k,m} = f_{i,j,k,m} r_{j,k,m}. \tag{12}
$$

### C. DSC Coverage Model

For a DSC deployed at $v_{j,k}$, the effective coverage mainly depends on LoS probability and the path-loss threshold in free space [9], [11], satisfying

$$
\begin{cases} P_{\mathrm{LoS}}(z_k, d_{i,j}) > \xi_{\mathrm{LoS}} \\ \dfrac{4\pi\rho \sqrt{z_k^2 + d_{i,j}^2}}{c} < \tau_{\mathrm{DU}}. \end{cases} \tag{13}
$$

In (13), $\xi_{\mathrm{LoS}}$ is the LoS probability threshold for D2V links and $\tau_{\mathrm{DU}}$ is the free space path-loss threshold, determined by the minimum signal-to-noise ratio for signal decoding.

Flight altitude determines the effective DSC coverage. Similar to the model in [20], the effective ground coverage radius of a DSC flying to a height of $z_k$ can be expressed as

$$
R_k = \min\left\{ \frac{z_k}{\tan(e_1 - \frac{1}{e_2} \ln \frac{1-\xi_{\mathrm{los}}}{e_1 \xi_{\mathrm{los}}})}, \sqrt{\left(\frac{c\tau_{\mathrm{DU}}}{4\pi\rho}\right)^2 - z_k^2} \right\}. \tag{14}
$$

Take Fig. 3 as an example to show the influence of flying height $z_k$ on $R_k$, where $e_1$, $e_2$, $\xi_{\mathrm{LoS}}$ and $\tau_{\mathrm{DU}}$ are set to 4.88, 0.43, 89dB, and 0.5, respectively. Note that the relationship between height and effective coverage radius is not linear.

### D. Traffic Model

We consider delay-sensitive traffic (e.g., rear-end collision avoidance, platooning/convoying). The average arrival rate and data packet length are denoted as $\lambda_a$ (packet/s) and $L_a$ (bit). The effective bandwidth theory [6], [18] is used to calculate the minimum transmission rate to guarantee that the downlink transmission delay exceeding $D^{(\mathrm{max})}$ at most probability $\varepsilon$, expressed as

$$
c^{(\mathrm{min})} = -\frac{L_a \log \varepsilon}{\log(1 - \frac{\log \varepsilon}{\lambda_a D^{(\mathrm{max})}}) D^{(\mathrm{max})}}. \tag{15}
$$

### III. PROBLEM FORMULATION

In the proposed spectrum management framework, the challenging issue is to determine the optimal spectrum slicing ratios and the association patterns to maximize the aggregate network utility while satisfying the QoS requirement of vehicular applications.

Let $\mathcal{I}_{j,k} = \{i \in \mathcal{I} | d_{i,j} \leq R_k\}$ be the set of vehicles located within the effective coverage of the DSC at $v_{j,k}$. If vehicle $i \in \mathcal{I}_{j,k}$ establishes a connection with the DSC at $v_{j,k}$, indication variable $a_{i,j,k}$ is set to 1; otherwise, 0. If a DSC at $v_{j,k}$ connects to GBS $m$, $b_{j,k,m}$ is set to 1; otherwise, set to 0. Once a DSC flies to GBSs' coverage area, it automatically connects to the GBS with the highest spectral efficiency.

A logarithmic function is applied to characterize the network utility with respect to the achievable transmission rate. Based on (9), the network utility achieved by all vehicles associated with the DSC at $v_{j,k}$ is expressed as

$$
u_{j,k}(\mathcal{A}_{j,k}, \mathcal{F}_{j,k})
$$
$$
= b_{j,k,1} \sum_{i \in \mathcal{I}_{j,k}} a_{i,j,k} \log(c_{i,j,k}^{(2)}) + b_{j,k,2} \sum_{i \in \mathcal{I}_{j,k}} a_{i,j,k} \log(c_{i,j,k}^{(1)})
$$
$$
+ b_{j,k,1} \sum_{i \in \mathcal{I}_{j,k}} a_{i,j,k} \log(c_{i,j,k}^{(3)}) + b_{j,k,2} \sum_{i \in \mathcal{I}_{j,k}} a_{i,j,k} \log(c_{i,j,k}^{(3)}) \tag{16}
$$

where $\mathcal{A}_{j,k} = \{a_{i,j,k} | i \in \mathcal{I}_{j,k}\}$, $\mathcal{B}_{j,k} = \{b_{j,k,m} | m \in \{1,2\}\}$, and $\mathcal{F}_{j,k} = \{f_{i,j,k}^{(n)} | i \in \mathcal{I}_{j,k}, n \in \{1,2,3\}, a_{i,j,k} = 1\}$. If vehicle $i$ connects to GBS $m$, indication variable $a_{i,m}$ is set to 1; otherwise, 0. The network utility achieved by all vehicles associated with GBS $m$ is expessed as

$$
u_m(\mathcal{A}_m, \mathcal{F}_m) = \sum_{i \in \mathcal{I}_m} a_{i,m} \log(c_{i,m}). \tag{17}
$$

where $\mathcal{A}_m = \{a_{i,m} | i \in \mathcal{I}_m\}$ and $\mathcal{F}_m = \{f_{i,m} | i \in \mathcal{I}_m, a_{i,m} = 1\}$. Given $\mathcal{A}_{j,k}$, the network utility at the DSC at $v_{j,k}$ to relay associated vehicles' traffic is calculated as

$$
u_{j,k,m}(\mathcal{A}_{j,k}, \mathcal{F}_{j,k,m}) = \sum_{i \in \mathcal{I}_{j,k}} a_{i,j,k} \log(c_{i,j,k,m}) \tag{18}
$$

with $\mathcal{F}_{j,k,m} = \{f_{i,j,k,m} | i \in \mathcal{I}_{j,k}, a_{i,j,k} = 1\}$.

Based on the logarithmic and linear utility functions, an aggregate utility maximization problem is formulated as in $\mathcal{P}1$ under the constraints of transmission rates, association

patterns, and resource partitioning.

$$\mathcal{P}1 : \underset{\substack{\alpha_1,\alpha_2,\alpha_3,\\ \mathcal{A}_{j,k},\mathcal{A}_m,\\ \mathcal{F}_{j,k},\mathcal{F}_m,\mathcal{F}_{j,k,m}}}{\text{Maximize}} \sum_{v_{j,k}\in\mathcal{V}_1\cup\mathcal{V}_2} u_{j,k}(\mathcal{A}_{j,k},\mathcal{F}_{j,k})$$

$$+ \sum_{m\in\{1,2\}} u_m(\mathcal{A}_m,\mathcal{F}_m) + \sum_{m\in\{1,2\}}\sum_{v_{j,k}\in\mathcal{V}_1\cup\mathcal{V}_2} u_{j,k,m}(\mathcal{A}_{j,k},\mathcal{F}_{j,k,m})$$

s.t.

$$a_{i,m}\left(c_{i,m} - c^{(\min)}\right) \geq 0, \forall i\in\mathcal{I}_m, \forall m\in\{1,2\} \quad (19a)$$

$$a_{i,j,k}\left(c_{i,j,k} - c^{(\min)}\right) \geq 0, \forall i\in\mathcal{I}_{j,k}, \forall v_{j,k} \quad (19b)$$

$$a_{i,j,k}\left(c_{i,j,k,m} - c^{(\min)}\right) \geq 0, \forall i\in\mathcal{I}_{j,k}, \forall v_{j,k} \quad (19c)$$

$$\sum_{m\in\{1,2\}} a_{i,m} + \sum_{m\in\{1,2\}}\sum_{v_{j,k}\in\mathcal{V}_m} a_{i,j,k} = 1 \quad (19d)$$

$$\sum_{i\in\mathcal{I}_{j,k}} a_{i,j,k}f_{i,j,k}^{(n)} - \alpha_n = 0, \forall v_{j,k}, \forall n\in\{1,2,3\} \quad (19e)$$

$$\sum_{i\in\mathcal{I}_m} a_{i,m}f_{i,m} = \delta_m W, \forall m \quad (19f)$$

$$\sum_{i\in\mathcal{I}_{j,k}} a_{i,j,k}f_{i,j,k,m} - \delta_{j,k,m} = 0, \forall v_{j,k} \quad (19g)$$

$$a_{i,j,k}, a_{i,m} \in \{0,1\}, \forall i\in\mathcal{I}_{j,k}, \forall v_{j,k} \quad (19h)$$

$$\sum_{m\in\{1,2\}}\left(\delta_m + \sum_{v_{j,k}\in\mathcal{V}_m}\delta_{j,k,m}\right) + \alpha_3 = 1 \quad (19i)$$

$$\alpha_n, \delta_m, \delta_{j,k,m} \in [0,1], \forall v_{j,k}, n\in\{1,2,3\} \quad (19j)$$

$$f_{i,j,k}^{(n)} \in (0,1), \forall i\in\mathcal{I}_{j,k}, \forall v_{j,k}, \forall n\in\{1,2,3\} \quad (19k)$$

$$f_{i,m} \in (0,1), \forall i\in\mathcal{I}_m, \forall m \quad (19l)$$

$$f_{i,j,k,m} \in (0,1), \forall i\in\mathcal{I}_{j,k}, \forall v_{j,k} \quad (19m)$$

The objective function of $\mathcal{P}1$ is the summation of utilities achieved by all vehicles (as receivers) and DSCs (as relays). Constraints (19a), (19b), and (19c) ensure that the achievable transmission rate at each receiver is not less than $c^{(\min)}$. Constraint (19d) ensures that each DSC can only connect to one BS. Constraints (19e)-(19g) state the resource allocation requirements for each DSC and GBS. Constraint (19i) is a combination of (1) and (2), reflecting the resource slicing requirement. Constraints (19k)-(19m) demonstrate the requirements on resource allocation for each vehicle.

$\mathcal{P}1$ contains a nonlinear objective function and constraints, belonging to a mixed-integer nonlinear programming problem. The vehicle association patterns depend on the DSC deployment and spectrum slicing ratios. Simultaneously, each vehicle's spectrum allocation rely on association patterns and spectrum slicing ratios, making problem-solving very difficult. For tractability, we first determines the optimal fractions of bandwidth resources, $f_{i,j,k}^{(n)}$, $f_{i,m}$, and $f_{i,j,k,m}$ given $\alpha_3$, $\delta_m$, and $\delta_{j,k,m}$.

## IV. SPECTRUM PARTITIONING SOLUTION

### A. Problem Approximation

We simplify $\mathcal{P}1$ by expressing $f_{i,j,k}^{(n)}$, $f_{i,m}$, and $f_{i,j,k,m}$ as a function of association indication variable $a_{i,j,k}$ to reduce the number of decision variables. The fractions of resources allocated to vehicles from the associated GBSs/DSCs are equal partitioning, expressed as

$$\begin{cases} f_{i,j,k}^{(n)*} = \dfrac{a_{i,j,k}\alpha_n W}{\sum_{i'\in\mathcal{I}_{j,k}} a_{i',j,k}} \triangleq f_{j,k}^{(n)*}(n\in\{1,2,3\}) \\[2ex] f_{i,m}^* = \dfrac{a_{i,m}\delta_m W}{\sum_{i'\in\mathcal{I}_m} a_{i',m}} \triangleq f_m^* \\[2ex] f_{i,j,k,m}^* = \dfrac{a_{i,j,k}\delta_{j,k,m}W}{\sum_{i'\in\mathcal{I}_{j,k}} a_{i',j,k}} \triangleq f_{j,k,m}^*. \end{cases} \quad (20)$$

Given $\mathcal{F}_{j,k}^* = \{f_{i,j,k}^{(n)*}|i\in\mathcal{I}_{j,k}, n\in\{1,2,3\}, a_{i,j,k}=1\}$, $\mathcal{F}_m^* = \{f_{i,m}^*|i\in\mathcal{I}_m, a_{i,m}=1\}$, and $\mathcal{F}_{j,k,m}^* = \{f_{i,j,k,m}^*|i\in\mathcal{I}_{j,k}, a_{i,j,k}=1\}$, we have

$$\begin{cases} u_{j,k}(\mathcal{A}_{j,k},\mathcal{F}_{j,k}^*) \triangleq u_{j,k}(\mathcal{A}_{j,k}) \\ u_m(\mathcal{A}_m,\mathcal{F}_m^*) \triangleq u_m(\mathcal{A}_m) \\ u_{j,k,m}(\mathcal{A}_{j,k},\mathcal{F}_{j,k,m}^*) \triangleq u_{j,k,m}(\mathcal{A}_{j,k}). \end{cases} \quad (21)$$

Based on (20) and (21), we reformulate $\mathcal{P}1$ as $\mathcal{P}2$.

$$\mathcal{P}2 : \underset{\substack{\alpha_1,\alpha_2,\alpha_3,\\ \mathcal{A}_{j,k},\mathcal{A}_m}}{\text{Maximize}} \sum_{v_{j,k}\in\mathcal{V}_1\cup\mathcal{V}_2} u_{j,k}(\mathcal{A}_{j,k}) + \sum_{m\in\{1,2\}} u_m(\mathcal{A}_m)$$

$$+ \sum_{v_{j,k}\in\mathcal{V}_1\cup\mathcal{V}_2} u_{j,k,m}(\mathcal{A}_{j,k})$$

s.t.

$$a_{i,m}\left(f_m^* r_{i,m} - c^{(\min)}\right), \forall i\in\mathcal{I}_m, \forall m \quad (22a)$$

$$a_{i,j,k}(b_{j,k,1}f_{i,j,k}^{(2)*}r_{i,j,k}^{(2)} + b_{j,k,2}f_{i,j,k}^{(1)*}f_{i,j,k}^{(1)}$$
$$+ b_{j,k,1}f_{i,j,k}^{(3)*}r_{i,j,k}^{(3)} + b_{j,k,2}f_{i,j,k}^{(3)*}r_{i,j,k}^{(3)} \quad (22b)$$
$$- c^{(\min)}) \geq 0, \forall i\in\mathcal{I}_{j,k}, \forall v_{j,k}, \forall n$$

$$a_{i,j,k}\left(f_{j,k,m}^* r_{j,k,m} - c^{(\min)}\right) \geq 0,$$
$$\forall i\in\mathcal{I}_{j,k}, \forall v_{j,k}, m \quad (22c)$$

$$(19h), (19i), (19j) \quad (22d)$$

Since $\{\mathcal{F}_{j,k},\mathcal{A}_{j,k}\}$, $\{\mathcal{F}_m,\mathcal{A}_m\}$, and $\{\mathcal{F}_{j,k,m},\mathcal{A}_{j,k}\}$ are coupled under (19i), it is feasible to transform $\mathcal{P}2$ into a tractable form.

### B. Problem Transformation

To solve $\mathcal{P}2$, we relax 0-1 variables in sets $\mathcal{A}_{j,k}$ and $\mathcal{A}_m$ to real-valued variables contained in $\widetilde{\mathcal{A}}_{j,k} = \{\widetilde{a}_{i,j,k}|i\in\mathcal{I}_{j,k}\}$ and $\widetilde{\mathcal{A}}_m = \{\widetilde{a}_{i,m}|i\in\mathcal{I}_m\}$, with $\widetilde{a}_{i,j,k}\in[0,1]$ and $\widetilde{a}_{i,m}\in[0,1]$. $\widetilde{a}_{i,m}$ is $a_{i,m}$ with $a_{i,j,k}$ substituted by $\widetilde{a}_{i,j,k}$. $\widetilde{a}_{i,j,k}$ and $\widetilde{a}_{i,m}$ can be considered as the probability of establishing the vehicle association in each spectrum slicing period [18].

*Proposition 1:* Functions $u_{j,k}(\mathcal{F}_{j,k},\widetilde{\mathcal{A}}_{j,k})$, $u_m(\mathcal{F}_m,\widetilde{\mathcal{A}}_m)$, and $u_{j,k,m}(\mathcal{F}_{j,k,m},\widetilde{\mathcal{A}}_{j,k})$ are biconcave on decision variable set $\{\mathcal{F}_{j,k},\mathcal{F}_m,\mathcal{F}_{j,k,m}\}\times\{\widetilde{\mathcal{A}}_{j,k},\widetilde{\mathcal{A}}_m\}$.

With the variable relaxation, $\mathcal{P}2$ is transformed to $\mathcal{P}3$.

$$\mathcal{P}3 : \underset{\substack{\alpha_1,\alpha_2,\alpha_3,\\ \widetilde{\mathcal{A}}_{j,k},\widetilde{\mathcal{A}}_m}}{\text{Maximize}} \sum_{v_{j,k}\in\mathcal{V}_1\cup\mathcal{V}_2} u_{j,k}(\widetilde{\mathcal{A}}_{j,k}) + \sum_{m\in\{1,2\}} u_m(\widetilde{\mathcal{A}}_m)$$

$$+ \sum_{m\in\{1,2\}}\sum_{v_{j,k}\in\mathcal{V}_1\cup\mathcal{V}_2} u_{j,k,m}(\widetilde{\mathcal{A}}_{j,k})$$

$$\text{s.t.}\begin{cases}\widetilde{a}_{i,m}\left(\widetilde{f}_m^* r_{i,m}-c^{(\min)}\right)\geq 0, \forall i\in\mathcal{I}_m, \forall m & (23a)\\[4pt]\widetilde{a}_{i,j,k}(b_{j,k,1}\widetilde{f}_{j,k}^{(2)*}r_{i,j,k}^{(2)}+b_{j,k,2}\widetilde{f}_{j,k}^{(1)*}r_{i,j,k}^{(1)}\\[4pt]\quad+b_{j,k,1}\widetilde{f}_{j,k}^{(3)*}r_{i,j,k}^{(3)}+b_{j,k,2}\widetilde{f}_{j,k}^{(3)*}r_{i,j,k}^{(3)}-c^{(\min)})(23b)\\[4pt]\quad\geq 0, \forall i\in\mathcal{I}_{j,k}, \forall v_{j,k}, \forall m, \forall n\\[4pt]\widetilde{a}_{i,j,k}\left(\widetilde{f}_{j,k,m}^* r_{j,k,m}-c^{(\min)}\right)\\[4pt]\quad\geq 0, \forall i\in\mathcal{I}_{j,k}, \forall v_{j,k}, \forall m & (23c)\\[4pt]\widetilde{a}_{i,m},\widetilde{a}_{i,j,k}\in[0,1], \forall i\in\mathcal{I}_{j,k}, \forall v_{j,k}, \forall m & (23d)\\[4pt](19i), (19j) & (23e)\end{cases}$$

Constraints (23a)-(23b) belong to linear inequality constraint functions, and constraint (23d) is a affine equality constraint function. Constraint (23a) actually indicates that if the DSC at $v_{j,k}$ is associated with GBS $m$ with $a_{i,m}=1$, the spectrum resource allocation for the vehicle should satisfy

$$a_{i,m}r_{i,m}\geq c^{(\min)}\sum_{i'\in\mathcal{I}_m}\widetilde{a}_{i',m}. \qquad (24)$$

Constraints (23b) and (23c) indicate that if $a_{i,j,k}=1$, the vehicle's resource allocation should satisfy

$$a_{i,j,k}r_{i,j,k}^{(n)}\geq c^{(\min)}\sum_{i'\in\mathcal{I}_{j,k}}\widetilde{a}_{i',j,k} \qquad (25)$$

and

$$b_{j,k,1}a_{i,j,k}r_{i,j,k}^{(2)}+b_{j,k,2}a_{i,j,k}r_{i,j,k}^{(1)}+b_{j,k,1}a_{i,j,k}r_{i,j,k}^{(3)}\\+b_{j,k,2}a_{i,j,k}r_{i,j,k}^{(3)}\geq c^{(\min)}\sum_{i'\in\mathcal{I}_{j,k}}\widetilde{a}_{i',j,k}. \qquad (26)$$

(24), (25), and (26) in $\mathcal{P}3$ indicate the lowest upper bound on the number of vehicles that can be associated with GBSs/DSCs given $\{\alpha_1,\alpha_2,\alpha_3\}$.

### C. Algorithm Design

The following corollaries, proved in B and C, summarize the concavity property of $\mathcal{P}3$.

*Corollary 1:* The objective function of $\mathcal{P}3$ is a biconcave function on variable set $\mathcal{F}\times\widetilde{\mathcal{A}}$, where $\mathcal{F}$ represents the set of all $\mathcal{F}_{j,k}$, $\mathcal{F}_m$, and $\mathcal{F}_{j,k,m}$ and $\widetilde{\mathcal{A}}$ the set of all $\widetilde{A}_{j,k}$ and $\widetilde{A}_m$.

*Corollary 2:* Algorithm 1 can converge to a set of optimal solutions $\{\alpha_1^*,\alpha_2^*,\alpha_3^*\}$, $\mathcal{F}^*$ and $\widetilde{\mathcal{A}}^*$.

By exploring the bi-concavity, we develop an alternate search algorithm to solve $\mathcal{P}3$, summarized in Algorithm 1. The main logic is to iteratively solve optimal association patterns $\widetilde{\mathcal{A}}^*$ and optimal spectrum slicing ratios $\{\alpha_1^*,\alpha_2^*,\alpha_3^*\}$ to maximize the objective function value. In the $(t+1)$th iteration, given a spectrum slicing ratio set, $\{\alpha_1^{(t)},\alpha_2^{(t)},\alpha_3^{(t)}\}$, and an association pattern set, $\widetilde{\mathcal{A}}^{(t)}$, from the $t$th iteration, $\mathcal{P}3$ is solved for $\Theta_m^{(t)}=\{\delta_m^{(t)},\delta_{j_1,k_1,m}^{(t)},\delta_{j_2,k_2,m}^{(t)},\ldots,\delta_{j_V,k_V,m}^{(t)}\}$, to find a better association pattern set, $\widetilde{\mathcal{A}}^\dagger$ with $\mathcal{F}$. Let $u^{(t)}$ denote the maximum objective function value with $\widetilde{\mathcal{A}}^{(t)}$ at the beginning of $t$th iteration. If the difference between $u^{(t+1)}$ and $u^{(t)}$ is less than threshold $\vartheta$, the iteration stops, and the algorithm converges to a set of optimal solutions, $\alpha_3^*$, $\Theta_1^*$, $\Theta_2^*$,

and $\widetilde{\mathcal{A}}^*$; otherwise, start the next iteration until it converges. As stated in Corollary 2, the algorithm can converges.

---

**Algorithm 1:** alternate_search_algorithm

**Input** : $\vartheta$; Candidate set for $\{\alpha_1,\alpha_2,\alpha_3\}$.
**Output**: Optimal spectrum slicing ratios $\{\alpha_1^*,\alpha_2^*,\alpha_3^*\}$ with $\Theta_m^*=\{\delta_m^*,\delta_{j_1,k_1,m}^*,\delta_{j_2,k_2,m}^*,\ldots,\}$ split from $\alpha_m^*$ ($m\in\{1,2\}$); Optimal association pattern set $\widetilde{\mathcal{A}}^*$.

1  $t\leftarrow 0$; $u^{(t)}\leftarrow 0$; $u^{(t+1)}\leftarrow 0$;
2  **while** $||u^{(t+1)}-u^{(t)}||\geq\vartheta$ **do**
3     Initialize candidate values for $\Theta_m$ and $\Theta_{j,k,m}$ given $\alpha_m^{(t)}$ ($m\in\{1,2\}$) and $\widetilde{\mathcal{A}}^{(t)}$;
4     $\Theta_1^{(t)}$ and $\Theta_2^{(t)}\leftarrow$ Solving $\mathcal{P}3$ given $\widetilde{\mathcal{A}}^{(t)}$ and $\{\alpha_1^{(t)},\alpha_2^{(t)},\alpha_3^{(t)}\}$.
5     $\widetilde{\mathcal{A}}^\dagger\leftarrow$ Solving $\mathcal{P}3$ given $\alpha_3^{(t)}$, $\Theta_1^{(t)}$, and $\Theta_2^{(t)}$;
6     Obtain $\mathcal{F}^\dagger$ given $\widetilde{\mathcal{A}}^\dagger$, $\alpha_3^{(t)}$, $\Theta_1^{(t)}$, and $\Theta_2^{(t)}$;
7     **if** *No solutions for $\mathcal{P}3$* **then**
8        Reinitialize until no solutions found; Break;
9     **else**
10       $\widetilde{\mathcal{A}}^{(t+1)}\leftarrow\widetilde{\mathcal{A}}^\dagger$;
11       $\alpha_3^\dagger$, $\Theta_1^\dagger$, and $\Theta_2^\dagger\leftarrow$ solving $\mathcal{P}3$ given $\widetilde{\mathcal{A}}^{(t+1)}$;
12       Obtain $\mathcal{F}^\dagger$ given $\widetilde{\mathcal{A}}^{(t+1)}$, $\alpha_3^\dagger$, $\Theta_1^\dagger$, and $\Theta_2^\dagger$;
13       **if** *No solutions for $\mathcal{P}3$* **then**
14          Reinitialize until no solutions found; Break;
15       **else**
16          $\alpha_3^{(t+1)}\leftarrow\alpha_3^\dagger$;
17          $\Theta_1^{(t+1)}$ and $\Theta_2^{(t+1)}\leftarrow\Theta_1^\dagger$ and $\Theta_2^\dagger$;
18          $\mathcal{F}^{(t+1)}\leftarrow\mathcal{F}^\dagger$;
19          Obtain $u^{(t+1)}$ with $\alpha_3^{(t+1)}$, $\Theta_1^{(t+1)}$, $\Theta_2^{(t+1)}$, $\widetilde{\mathcal{A}}^{(t+1)}$ and $\mathcal{F}^{(t+1)}$ at the $t$th iteration;
20       $t\leftarrow t+1$;

---

### V. PERFORMANCE EVALUATION

Extensive simulation is carried out to verify the effectiveness of the proposed solution. The proposed scheme is categorized as versions I and II. The former is a full-featured version with flight altitude adaptation as in [20], while the latter does not allow DSCs to reuse GBSs' spectrum resources. For comparison, we provide two baseline schemes:

- **Maximization-SINR (max-SINR) scheme** [10], in which the DSC deployment with flight altitude adaptation aims to maximize the aggregate spectrum efficiency;
- **Maximization-DSC-coverage (max-Cov) scheme** [11], in which each DSC always maintains the height that maximizes the effective coverage.

Each baseline is further categorized as versions I and II. The former uses the same dynamic DSC deployment as the proposed scheme, while the latter is with static deployment.
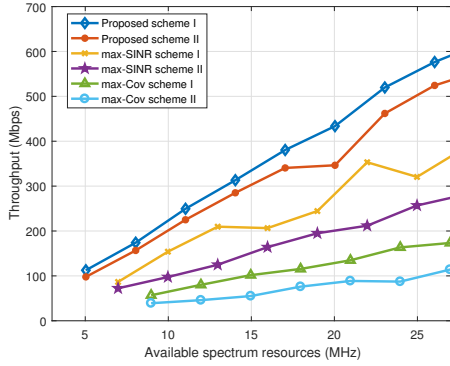
Fig. 4. Impact of spectrum resources on different schemes.
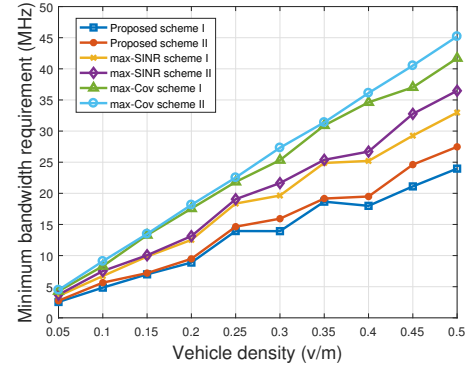


Fig. 5. Impact of vehicle density on different schemes.
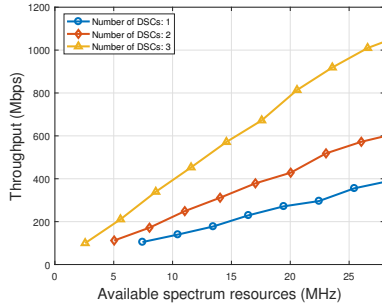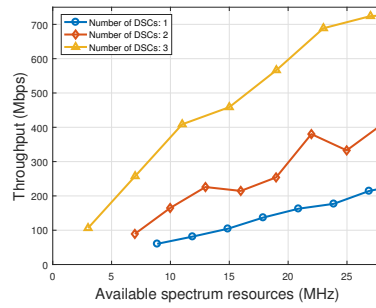


(a) Proposed scheme I     (b) max-SINR scheme I     (c) max-Cov scheme I
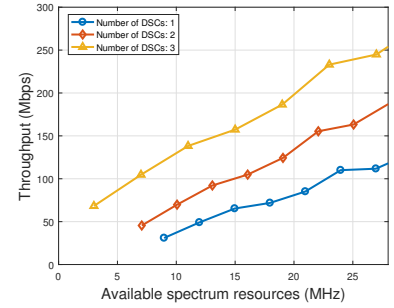
Fig. 6. Impact of the number of DSCs.

TABLE I
PARAMETER SETTINGS

| Parameters | Values |
|---|---|
| GBS altitude $m$ ($z_m$) | 10m |
| Coverage radius of each GBS ($R_m$) | 800m |
| Transmit power of GBS $m$ ($p_m$) | 46dBm |
| Transmit power of the DSC at $v_{j,k}$ ($p_{j,k}$) | 24dBm |
| Urban environment parameter ($e_1/e_2$) | 4.88/0.43 |
| Excess pathloss scalar/angle scalar($o_1/o_2$) | -23.29/4.14 |
| Additional loss for LoS/NLoS links ($\eta_{\text{LoS}}/\eta_{\text{NLoS}}$) | 0.1/21 |
| Terrestrial path-loss exponent ($\gamma$) | 3.04 |
| Angle offset ($\theta_0$) | 3.61 |
| Excess path-loss offset ($\eta_0$) | 20.7 |
| Carrier frequency ($f$) | 3.5GHz |
| LoS probability threshold for D2V links ($\xi_{\text{LoS}}$) | 0.5 |
| Free space path-loss threshold ($\tau_{\text{DU}}$) | 89dB |
| Packet arrival rate ($\lambda_a$) | 4pkt/s |
| Packet length ($L_a$) | 1048bit |
| Packet delay bound ($D^{(\max)}$) | 0.001s |
| Delay bound violation probability ($\varepsilon$) | $10^{-3}$ |
| Stop criterion ($\vartheta$) | 0.01 |

Consider a scenario with two adjacent GBSs and multiple DSCs. The DSC flying height range on each x-y plane coordinate is [0, 200m] with an adjacent height interval of 10m, and the horizontal movement range on the x-y coordinate

plane is set to [-1600m,1600m]. Each lane's vehicle density range is set to [0.05, 0.5] v/m, where the minimum vehicle distance is 5m. Table I lists other important parameters.

**Impact of Available Spectrum Resources**: Fig. 4 compares the throughput (presented in the aggregate transmission rate) with two DSCs deployed. The average vehicle density is set to 0.1 v/m. With the increase of resources, the throughput of our scheme increases more rapidly than other schemes. Particularly, the proposed scheme's minimum spectrum resource requirement is 5MHz, while at least 7 MHz (8MHz) spectrum are required by the max-SINR (max-Cov) scheme. Due to efficient spectrum reuse, the throughput of our scheme is on average over 30% higher than that of the max-SINR scheme and over 45% higher on average than the max-Cov scheme.

**Impact of Vehicle Density**: Fig. 5 shows the performance on minimum spectrum resource consumption, where the amount of available spectrum resources is 20MHz. The proposed scheme's minimum resource consumption is on average over 15% lower than the max-SINR scheme and over 25% lower on average than the max-Cov scheme, with a slower increase trend with the increase of vehicle density.

**Impact of the Number of DSCs**: In Fig. 6, the starting point on the left side of the line represents the lower bound of resources required by different strategies under QoS constraints. With the increase in DSCs, more vehicles can connect to DSCs, and the overall spectrum utilization increases. Under

a given amount of resources, the proposed scheme achieves higher throughput than max-SINR and max-Cov schemes.

## VI. Conclusion

In this paper, we have proposed a spectrum management framework for air-ground integrated vehicular networks. The goal is to maximize network utility subject to QoS requirements. The network utility maximization problem is formulated to determine vehicle-DSC association patterns and spectrum partitioning among heterogeneous BSs. The optimization problem is further transformed into a tractable biconcave form, followed by an alternate search algorithm to obtain optimal spectrum slicing ratios and association patterns. Simulation results demonstrate the proposed method has advantages in throughput and spectrum utilization.

## Appendix

### A. Proof of Proposition 1

According to the property of the log function, we have

$$
\begin{aligned}
& b_{j,k,1} \sum_{i \in \mathcal{I}_{j,k}} \widetilde{a}_{i,j,k} \log(f_{j,k}^{(2)*} r_{i,j,k}^{(2)}) \\
&= b_{j,k,1} \sum_{i \in \mathcal{I}_{j,k}} \widetilde{a}_{i,j,k} \log(W \alpha_n r_{i,j,k}^{(n)}) \\
&\quad - b_{j,k,1} \sum_{i \in \mathcal{I}_{j,k}} \widetilde{a}_{i,j,k} \log \left( \sum_{i' \in \mathcal{I}_{j,k}} \widetilde{a}_{i',j,k} \right).
\end{aligned}
\tag{27}
$$

By stating an equation for the coefficients via indices $i_l$ and $i_{l'}$, we express the Hessian matrix of (27) for $\widetilde{\mathcal{A}}_{j,k}$ as

$$
\begin{aligned}
\mathbf{H}_{i_l, i_{l'}} &= \frac{\partial^2 \left( b_{j,k,1} \sum_{i \in \mathcal{I}_{j,k}} \widetilde{a}_{i,j,k} \log(f_{j,k}^{(2)*} r_{i,j,k}^{(2)}) \right)}{\partial \widetilde{a}_{i_l,j,k} \partial \widetilde{a}_{i_{l'},j,k}} \\
&= -\frac{1}{\sum_{i \in \mathcal{I}_{j,k}} \widetilde{a}_{i,j,k}}.
\end{aligned}
\tag{28}
$$

For any non-zero vector $\mathbf{s} = [s_1, s_2, \ldots, s_{I_{j,k}}] \in \mathbb{R}^{I_{j,k}}$, we have

$$
\mathbf{s}^T \mathbf{H}_{i_l, i_{l'}} \mathbf{s} = -\frac{\sum_{i \in \mathcal{I}_{j,k}} s_i^2}{\sum_{i \in \mathcal{I}_{j,k}} \widetilde{a}_{i,j,k}} \leq 0.
\tag{29}
$$

Since the Hessian matrix is negative definite, function $b_{j,k,1} \sum_{i \in \mathcal{I}_{j,k}} \widetilde{a}_{i,j,k} \log(f_{j,k}^{(2)*} r_{i,j,k}^{(2)})$ is concave with respect to $\widetilde{\mathcal{A}}_{j,k}$ for any given $\alpha_3$, and the reverse is also true.

The proof for $u_{j,k,m}(\widetilde{\mathcal{A}}_{i,j,k})$ and $u_m(\widetilde{\mathcal{A}}_m)$ are similar.

### B. Proof of Corollary 1

The objective function of $\mathcal{P}3$ is a nonnegative linear combination of a set of biconcave functions, which also belongs to a biconcave function on variable set $\mathcal{F} \times \widetilde{\mathcal{A}}$ [21].

### C. Proof of Corollary 2

Both $\mathcal{F} \times \widetilde{\mathcal{A}}$ are closed sets, and the objective function of $\mathcal{P}3$ is continuous on its domain. To verify the uniqueness of $\mathcal{F}^{(t+1)}$ and $\widetilde{\mathcal{A}}^{(t+1)}$ at the end of the $t$-th iteration, we refer to the proof of Corollary 1 that, given $\mathcal{F}$, the objective function

of $\mathcal{P}4$ is a concave function of $\widetilde{\mathcal{A}}$. Conversely, given $\widetilde{\mathcal{A}}$, the objective function is also a concave function in terms of $\Theta$. Therefore, Algorithm 1 can converge to $\mathcal{F}^*$ and $\widetilde{\mathcal{A}}^*$.

## References

[1] W. Zhuang, Q. Ye, F. Lyu, N. Cheng, and J. Ren, "SDN/NFV-empowered future IoV with enhanced communication, computing, and caching," *Proc. IEEE*, vol. 108, no. 2, pp. 274–291, 2020.

[2] S. Chen, J. Hu, Y. Shi, L. Zhao, and W. Li, "A vision of C-V2X: Technologies, field testing, and challenges with chinese development," *IEEE Internet Things J.*, vol. 7, no. 5, pp. 3872–3881, 2020.

[3] B. Shang, Y. Yi, and L. Liu, "Computing over space-air-ground integrated networks: Challenges and opportunities," *IEEE Netw.*, vol. 35, no. 4, pp. 302–309, 2021.

[4] W. Shi, J. Li, N. Cheng, F. Lyu, and X. Shen, "Multi-drone 3D trajectory planning and scheduling in drone assisted radio access networks," *IEEE Trans. Veh. Technol.*, vol. 68, no. 8, pp. 8145–8158, 2019.

[5] J. Liu and N. Kato, "A markovian analysis for explicit probabilistic stopping-based information propagation in postdisaster ad hoc mobile networks," *IEEE Trans. Wireless Commun.*, vol. 15, no. 1, pp. 81–90, 2015.

[6] H. Peng, Q. Ye, and X. Shen, "Spectrum management for multi-access edge computing in autonomous vehicular networks," *IEEE Trans. Intell. Transp. Syst.*, vol. 21, no. 7, pp. 3001–3012, 2020.

[7] H. Peng and X. Shen, "Multi-agent reinforcement learning based resource management in MEC- and UAV-assisted vehicular networks," *IEEE J. Sel. Area. Comm.*, vol. 39, pp. 131–141, 2021.

[8] Q. Ye, W. Shi, K. Qu, H. He, W. Zhuang, and X. Shen, "Joint ran slicing and computation offloading for autonomous vehicular networks: A learning-assisted hierarchical approach," *IEEE Open J. Veh. Technol.*, vol. 2, pp. 272–288, 2021.

[9] A. Al-Hourani, S. Kandeepan, and S. Lardner, "Optimal LAP altitude for maximum coverage," *IEEE Wireless Commun. Lett.*, vol. 3, no. 6, pp. 569–572, 2014.

[10] X. Sun and N. Ansari, "Jointly optimizing drone-mounted base station placement and user association in heterogeneous networks," in *IEEE ICC*, 2018, pp. 1–6.

[11] W. Shi, J. Li, W. Xu, H. Zhou, N. Zhang, S. Zhang, and X. Shen, "Multiple drone-cell deployment analyses and optimization in drone assisted radio access networks," *IEEE Access*, vol. 6, pp. 12 518–12 529, 2018.

[12] Y. Li and L. Cai, "UAV-assisted dynamic coverage in a heterogeneous cellular system," *IEEE Netw.*, vol. 31, no. 4, pp. 56–61, 2017.

[13] N. Zhang, S. Zhang, P. Yang, O. Alhussein, and X. Shen, "Software defined space-air-ground integrated vehicular networks: Challenges and solutions," *IEEE Commun. Mag.*, vol. 55, no. 7, 2017.

[14] Y. He, D. Zhai, Y. Jiang, and R. Zhang, "Relay selection for uav-assisted urban vehicular ad hoc networks," *IEEE Wireless Commun. Lett.*, 2020.

[15] H. Wu, J. Chen, C. Zhou, W. Shi, N. Cheng, W. Xu, W. Zhuang, and X. S. Shen, "Resource management in space-air-ground integrated vehicular networks: SDN control and AI algorithm design," *IEEE Wireless Commun.*, vol. 27, no. 6, pp. 52–60, 2020.

[16] F. Lyu, P. Yang, H. Wu, C. Zhou, J. Ren, Y. Zhang, and X. Shen, "Service-oriented dynamic resource slicing and optimization for space-air-ground integrated vehicular networks," *IEEE Trans. Intell. Transp. Syst.*, 2021, DOI:10.1109/TITS.2021.3070542.

[17] Q. Duan, N. Ansari, and M. Toy, "Software-defined network virtualization: An architectural framework for integrating SDN and NFV for service provisioning in future networks," *IEEE Netw.*, vol. 30, no. 5, pp. 10–16, 2016.

[18] Q. Ye, W. Zhuang, S. Zhang, A.-L. Jin, X. Shen, and X. Li, "Dynamic radio resource slicing for a two-tier heterogeneous wireless network," *IEEE Trans. Veh. Technol.*, vol. 67, no. 10, pp. 9896–9910, 2018.

[19] A. Al-Hourani and K. Gomez, "Modeling cellular-to-UAV path-loss for suburban environments," *IEEE Wireless Commun. Lett.*, vol. 7, no. 1, pp. 82–85, 2018.

[20] H. Shen, Q. Ye, W. Zhuang, W. Shi, G. Bai, and G. Yang, "Drone-small-cell-assisted resource slicing for 5G uplink radio access networks," *IEEE Trans. Veh. Technol.*, vol. 70, no. 7, pp. 7071–7086, 2021.

[21] J. Gorski, F. Pfeuffer, and K. Klamroth, "Biconvex sets and optimization with biconvex functions: a survey and extensions," *Math. Meth. Oper. Res.*, vol. 66, no. 3, pp. 373–407, 2007.